Electrochimica Acta 68 (2012) 246–253

Contents lists available at SciVerse ScienceDirect

Electrochimica Acta

journal homepage: www.elsevier.com/locate/electacta

Electrochemical performance of cobalt free, $Li_{1.2}(Mn_{0.32}Ni_{0.32}Fe_{0.16})O_2$ cathodes for lithium batteries

K. Karthikeyan [a], S. Amaresh [a], G.W. Lee [a], V. Aravindan [a,b], H. Kim [c], K.S. Kang [c], W.S. Kim [d], Y.S. Lee [a,*]

[a] Faculty of Applied Chemical Engineering, Chonnam National University, Gwang-ju 500-757, Republic of Korea
[b] Energy Research Institute (ERI@N), Nanyang Technological University, Research Techno Plaza, 50 Nanyang Drive, Singapore 637553, Singapore
[c] Department of Materials Science and Engineering, Seoul National University, Seoul 151-742, Republic of Korea
[d] Daejung EM Co. Ltd, Incheon 405-820, Republic of Korea

ARTICLE INFO

Article history:
Received 29 November 2011
Received in revised form 21 February 2012
Accepted 21 February 2012
Available online 1 March 2012

Keywords:
Layered materials
$Li_{1.2}(Mn_{0.32}Ni_{0.32}Fe_{0.16})O_2$
Cobalt free cathodes
Li_2MnO_3
Solid solution

ABSTRACT

Cobalt free, eco-friendly layered $Li_{1.2}(Mn_{0.32}Ni_{0.32}Fe_{0.16})O_2$ compounds were synthesized using the adipic acid assisted sol–gel method. The structure and morphology of the prepared materials were examined by X-ray diffraction (XRD), scanning electron microscopy (SEM) and transmission electron microscopy (TEM). The XRD results revealed that all of the materials possess a layered α-$NaFeO_2$ structure with $R\bar{3}m$ space group. The TEM images confirmed the presence of carbon on the surface of the synthesized material. Galvanostatic charge/discharge studies demonstrated that the cyclic performance and rate capability of the materials were improved by the presence of carbon and the crystalline nature of the material. Among the synthesized materials, the sample prepared with 1 M adipic acid exhibited not only a high discharge capacity of 160 mAh g^{-1}, but also excellent cycling performance with a capacity retention of over 92% after 25 cycles. In addition, electrochemical impedance spectroscopy (EIS) was used to confirm the improvement in the electronic conductivity and the results are discussed in detail.

1. Introduction

Lithium ion batteries (LIBs) have become the predominant power sources for consumer electronic devices, such as cellular phones, and laptops, due to their high energy density, long cycle life and light weight. However, their limited high rate capability has restricted their use in electric vehicle applications, which are being considered to solve issues such as air pollution combined with the foreseen oil shortage. Although $LiCoO_2$ has been commercialized as a cathode material in practical LIBs, numerous attempts had been made to find an appropriate alternative candidate, due to the high cost, toxicity and instability of cobalt at high potential windows greater than 4.3 V [1,2]. The layered materials, $LiNiO_2$ and $LiMnO_2$, have been extensively studied as an alternative for $LiCoO_2$, but they possess various practical limitations, such as the difficulty to synthesize phase pure materials, structural changes during cycling, thermal instability of $LiNiO_2$ and structural degradation of $LiMnO_2$, leading to poor electrochemical performance [3–5]. Meanwhile, candidates such as $LiMn_2O_4$ and $LiFePO_4$ have also been proposed and widely investigated. However, the former suffers from problems during operation at elevated temperatures, because of the possible Mn^{3+} dissolution and subsequent attack on the counter electrode, which deteriorates the performance of the cell. The latter is affected by its inherent conductivity issue, which restricts the rate performance of the cell and also limits the operating voltage (3.4 V vs. Li) of the electrode [6]. Hence, the search is still on for high performance cathodes, preferably with a layered structure, which can exceed the combined advantages of the existing cathodes with superior electrochemical performance, low cost and eco-friendly material.

Ohzuku et al. [7,8] proposed the new layered materials, $LiNi_{1/2}Mn_{1/2}O_2$ and $LiNi_{1/3}Co_{1/3}Mn_{1/3}O_2$, which were synthesized by the co-precipitation method. Dahn et al. [9] reported that $Li[Ni_xMn_xCo_{1-2x}]O_2$ ($1/4 < x < 3/8$) materials delivered a discharge capacity of 160 mAh g^{-1}. Another Mn based material proposed as a possible alternate was Li_2MnO_3, but it was found to be electrochemically inactive and the capacity obtained was mainly due to the exchange of H^+ ions [10,11]. It was believed that the oxidation of Mn^{4+} to Mn^{5+} is not easier due to the tetravalent arrangement of Mn. At the same time, numerous studies have been devoted to the development of Mn based cathodes, due to its high specific capacity, low-cost and environmentally benign nature. To overcome the electrochemical inactivity of Li_2MnO_3, the concept of preparing a one to one solid state solution with other layered materials has been adopted. Recently, many solid state solutions have been widely studied, such as Li_2MnO_3–$LiMO_2$ (M = Ni, Cr and Co) [12–15], $LiNiO_2$–Li_2MnO_3–$LiCoO_2$ [16], Li_2MnO_3–$LiNi_{1-x}Co_xO_2$ [17], $LiNi_{0.5}Mn_{0.5}O_2$–Li_2MnO_3–$LiCoO_2$

* Corresponding author. Tel.: +82 62 530 1904; fax: +82 62 530 1904.
E-mail address: leeys@chonnam.ac.kr (Y.S. Lee).

0013-4686/$ – see front matter.
doi:10.1016/j.electacta.2012.02.076

[18], and Li_2MnO_3–$LiCo_{1/3}Ni_{1/3}Mn_{1/3}O_2$ [19]. Of late, layered materials containing lithium rich compositions, $Li(Li_xM_{1-x})O_2$, where M is Mn, Ni or Co have attracted the attention of researchers. For instance, Zhang et al. [13] and Shin et al. [20] demonstrated that Li–Mn–Ni–O materials with excess lithium delivered a much higher capacity than that of the stoichiometric composition, $LiMn_{0.5}Ni_{0.5}O_2$, due to the structural stabilization formed between the $LiMn_{0.5}Ni_{0.5}O_2$ and Li_2MnO_3 solid solutions. More recently, Ma et al. [21] also reported the preparation of an $Li_{1+z}(Mn_{0.4}Ni_{0.4}Co_{0.2})_{1-z}O_2$ solid solution without any secondary phase materials, unlike in the case of Li_2MnO_3.

The above-mentioned Li_2MnO_3 based solid solutions comprising Co and Cr doped materials exhibited good electrochemical performances, however, their high cost and relatively high toxicity, when compared to the native compound, have restricted their utilization in practical LIBs. Utilizing $LiFeO_2$ is thought to be the best way to reduce the cost and amount of toxic elements in such layered materials [22]. Recently, Tabuchi et al. [23,24] reported the development of iron based Li_2MnO_3 as a 4 V cathode material prepared using a combination of co-precipitation followed by hydrothermal reaction and, finally, the solid state method to synthesize these materials. The results suggested the possibility of using this new cathode material in the 4 V region, because of its unique $Fe^{4+/3+}$ redox couple at ~4 V. In spite of their apparently good structural properties, these materials exhibited poor cycle performance, due to their preparation method which involved three complicated steps and may affect their electrochemical performance. In addition, an oxidizer is used during the hydrothermal step, which increases the production cost as well. It is generally believed that the utilization of such a redox couple is impractical in layered type oxides, for example, $LiFeO_2$, Li_2MnO_3–$LiFeO_2$ solid solutions, etc. Of late, the preparation of "cobalt free" layered oxides comprising solid solutions of the type mentioned above was attempted with other transition metal elements such as Mn and Ni. This study sparked our motivation to develop Fe substituted layered cathode materials with improved electrochemical performance via simple synthesis routes such as the sol–gel or solid state methods, and to scale this procedure up further. In this connection, we prepared a layered manganese oxide solid solution of $Li_{1+x}(Mn_{0.4}Fe_{0.2}Ni_{0.4})_{1-x}O_2$ ($0 < x < 0.4$) materials with three end members, viz. Li_2MnO_3, $LiNiO_2$ and $LiFeO_2$, using a simple adipic acid assisted sol–gel technique. Although the optimization of the x value and calcination temperature was not discussed in this paper, the materials prepared with $x = 0.2$ ($Li_{1.2}(Mn_{0.32}Ni_{0.32}Fe_{0.16})O_2$) at 700 °C, which exhibited the best electrochemical properties among the compositions prepared, were described in detail. It is worth mentioning that the presence of di-carboxyl groups (COOH) in adipic acid effectively suppresses the particle growth during the synthesis procedure when compared to the other members of the group, such as oxalic acid, malonic acid, succinic acid, suberic acid and sebacic acid [25]. Furthermore, the powders obtained by the adipic acid assisted technique exhibited excellent hexagonal ordering and, moreover, sub-micron sized particles with a narrow particle-size distribution were observed for the $LiNi_{0.8}Co_{0.2}O_2$ system. In line with this research, we adopted adipic acid as a chelating agent and its influence on the electrochemical properties of $Li_{1.2}(Mn_{0.32}Ni_{0.32}Fe_{0.16})O_2$ are studied and described in detail.

2. Experimental

The sol–gel method was adopted to synthesize $Li_{1.2}(Mn_{0.32}Ni_{0.32}Fe_{0.16})O_2$ (LMNFO) using adipic acid (AA) as a chelating agent, though it can also act as source of carbon. In the present study, various molar ratios of adipic acid to total metal ions were used, viz. 0, 0.25, 0.5, 0.75 and 1 M. In the synthetic process, appropriate amounts of $Li(CH_3COO)_2{\cdot}H_2O$ (Wako, Japan), $Fe(CH_3COO)_2{\cdot}H_2O$ (Aldrich), $Ni(CH_3COO)_2{\cdot}4H_2O$ (Aldrich), and $Mn(CH_3COO)_2{\cdot}4H_2O$ (Aldrich) were dissolved in distilled water and then added to a continuously stirred aqueous solution containing $C_6H_{10}O_4$ (Sigma–Aldrich). The pH of the solution was kept neutral by incorporating ammonium hydroxide (NH_4OH) solution. The resultant solution was evaporated at 80 °C until a transparent sol was obtained. After the evaporation of water, the sol turned into a viscous transparent gel. The resulting gel precursors were decomposed at 400 °C for 4 h in air to eliminate the organic moieties, such as acetate and carboxylic groups. The decomposed powders were ground, pressed into pellets and fired at 700 °C for 10 h in an oxygen atmosphere to obtain nanocrystalline powders. The samples prepared with 0.25, 0.5, 0.75 and 1 M AA were named samples A, B, C and D, respectively.

The phase analysis of all of the synthesized powders was carried out by X-ray diffraction using Cu Kα radiation (XRD, Rint 1000 Regaku, Japan) with a scan speed of $2^\circ\ min^{-1}$ between 10 and 80° at an applied potential of 40 kV and current of 30 mA. The surface morphology of the powders was observed by scanning electron microscopy (SEM, S-4700 microscope, Hitachi, Japan) and transmission electron microscopy (TEM, TecnaiF20, Philips, Holland). Cyclic voltammetry (CV) and electrochemical impedance spectroscopy (EIS) studies were performed using an electrochemical analyzer (SP-150, Bio-Logic, France). A Micromeritics ASAP 2010 surface analyzer (Micromeritics, USA) was used to calculate the Brunauer–Emmett–Teller (BET) surface area of the prepared powders. The carbon content in the samples was determined by elemental analysis (Elementar Analysensysteme GmbH, Germany). Galvanostatic charge/discharge tests were performed using CR 2032 coin cells. The composite cathodes were prepared by pressing a mixture of accurately weighed samples consisting of 20 mg of the prepared material, 3 mg of Ketzen black and 3 mg of Teflonized acetylene black (TAB) on a 200 mm^2 stainless steel mesh and subsequently dried at 160 °C in a vacuum oven for 4 h. The test cell was fabricated in an argon filled glove box by pressing together the composite cathode and lithium metal anode separated by a porous polypropylene separator (Celgard 3401). 1 M $LiPF_6$ in 1:1 EC/DMC (Techno Semichem. Co. Ltd., Korea) was used as the electrolyte. The test cells were cycled at a constant current density of 0.1 mA cm^{-2} between 2 and 4.5 V at room temperature.

3. Results and discussion

Fig. 1 shows the XRD patterns of the LMNFO samples prepared with different molar ratios of AA synthesized at 700 °C. The well-defined narrow reflections indicate the good crystalline nature of the synthesized powders with various ratios of AA. Moreover, the intensity of the diffraction peaks gradually increased with increasing amount of AA, revealing the improvement in the crystalline nature of the sample with a high AA content. The peaks are indexed based on the hexagonal α-$NaFeO_2$ structure with a space group of $R\bar{3}m$, which indicates that the layer of lithium is substituted with a layer containing lithium, manganese, nickel and iron atoms [23]. In addition, the two super lattice peaks observed between 20 and 30°, caused by the short range ordering of Li, Ni, Mn and Fe in the 3*a* sites, indicate the existence of a layered structure with Li_2MnO_3 character [16]. However, these super lattice peaks were gradually suppressed as the adipic acid ratio increased. Further, the suppression of these peaks with increasing AA content also infers that the undetectable monoclinic phase of Li_2MnO_3 turns into the hexagonal layered rock-salt phase, which is in good agreement with the previous reports by Tabuchi et al. [23,24]. This is expected, because the incorporation of Fe^{3+} leads to the formation of the above solid solution, co-existing between α-$LiFeO_2$ and Li_2MnO_3 with the same layered structure. The lattice parameter values are calculated and given in Table 1. The integrated ratio of the $I_{(003)}/I_{(104)}$ peaks has

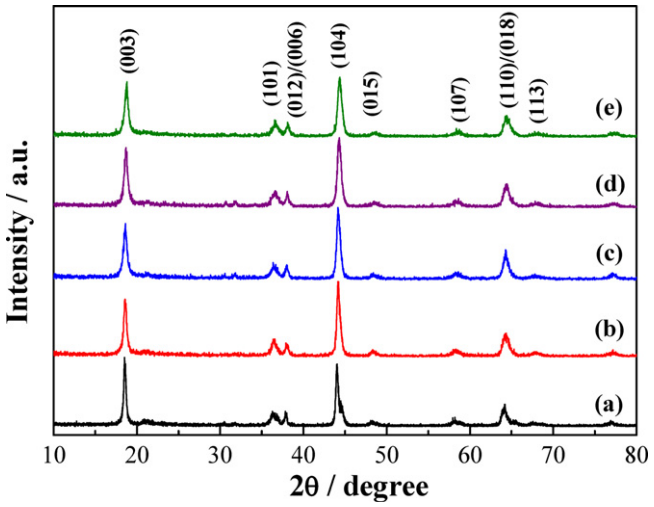

Fig. 1. XRD patterns of pristine and adipic acid assisted $Li_{1.2}(Mn_{0.32}Ni_{0.32}Fe_{0.16})O_2$ materials (a) pristine, (b) 0.25 M AA, (c) 0.5 M AA, (d) 0.75 M AA, and (e) 1 M AA concentrations.

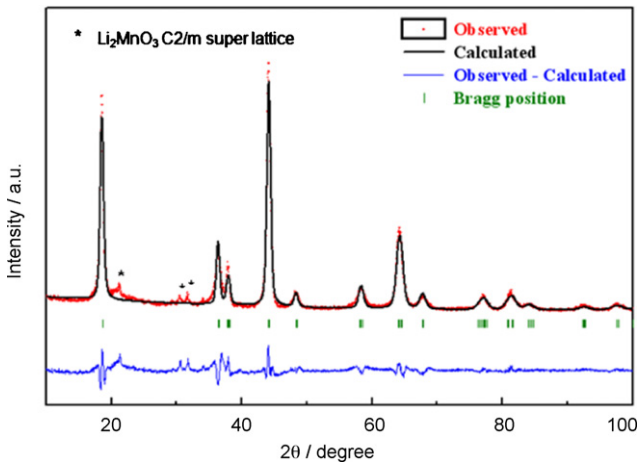

Fig. 2. Rietveld refinement pattern of 0.75 M adipic acid assisted $Li_{1.2}(Mn_{0.32}Ni_{0.32}Fe_{0.16})O_2$. The pattern was refined according to the $Li[Li_{0.2}Ni_{0.2}Mn_{0.6}]O_2$ structure.

been proposed to be a critical indication of the partial interchange of occupancy of the Li and transition metal ions among the sites, or so-called cation mixing [26]. The ratio of $I_{(003)}/I_{(104)}$ increases with increasing AA ratio from 0.75 to 0.94. This indicates that the cation mixing between Ni^{2+} and Li^+ is decreased, and the ratio observed for sample D was in good agreement with the reported values, which means that good electrochemical performance can be expected [7,8]. Generally, the *c*/*a* ratio is used to determine the hexagonality of a layered material and, when it is more than 4.9, the material possesses layered characteristics [16–18]. In our study, the *c*/*a* ratio determined for all of the samples is more than 4.9, which shows that they have well defined layered structural properties which would facilitate the diffusion of one dimensional Li^+ ion transport in the matrix.

The XRD pattern of sample C was further subjected to Rietveld refinement with respect to the $Li_{1.2}Ni_{0.2}Mn_{0.6}O_2$ phase and the results are presented in Fig. 2. The refinement was conducted based on the assumption that the Li-ions occupy the *3a* sites, Ni, Mn and Fe are located in the *3b* sites, and O is located in the *6c* sites. Consequently, an analysis was carried out to find the cation mixing of nickel in the lithium sites, because the radius of Ni^{2+} (0.69 Å) is close to that of Li^+ (0.76 Å). As can be seen from Fig. 2, the presence of superstructure peaks in the region of 20–33° resulted from the ordering of lithium and manganese in the transition metal layers. From the Rietveld analysis, the cation distribution of these layers can be written as $(Li_{0.925}Ni_{0.075})_{3a}[M_{0.726}Li_{0.275}]_{3b}O_2$. This clearly indicates that, for the composition of $Li_{1.2}(Mn_{0.32}Ni_{0.32}Fe_{0.16})O_2$, only 0.075 moles of the formula unit of Ni^{2+} were incorporated into the Li layer, which means that a low level of cation mixing occurred.

The SEM images of the pristine, A, B, C and D samples calcined at 700 °C are shown in Fig. 3. All of the samples exhibited a cluster of weakly aggregated particulates in the scanned area. There is a greater deal of agglomeration of non-uniform particles observed on the surface of the pristine sample. It can be clearly seen from the SEM images that as the content of AA increased, the tendency toward aggregation decreased. However, primary particles with a size of about 100–120 nm are observed for samples A (Fig. 3(b)) and B (Fig. 3(c)). It is well known that electrochemical lithium insertion/extraction is much easier in small size particles due to the reduction of diffusion pathways for Li^+ ions, which also enable faster electronic transport through their size effect. It was reported that polycrystalline materials with a grain size of up to 100 nm could exhibit enhanced diffusivity and a higher thermal co-efficient than conventional materials [27,28]. The materials with a higher AA content exhibit a slightly larger particle size with a more uniform size distribution. As the content of AA increased from 0.25 to 1 M, the size of the primary particles increased to about 200 nm. Furthermore, sample D (Fig. 3(e)) consisted of uniform large particles and a very small proportion of aggregation. The sample with a higher AA content exhibited somewhat suppressed particle agglomeration, but the average particle size is larger than that of the other AA treated samples, which is essential for good higher rate performance. Although the carbon coating cannot be clearly detected in Fig. 3, very small particles around 10–20 nm in size are bound on the surface of the LMNFO powders, especially at higher AA contents, and can be considered to be small carbon particles.

In order to confirm the presence of carbon, a TEM analysis was carried out for sample D (700 °C) and the results are presented in Fig. 4. It can be clearly seen from Fig. 4(a) and (b) that sample D has a uniform particle size distribution and small size residual carbon particles are also available, which is due to the carbonization of AA during the calcination process. The formation of nanosized materials may be ascribed to the sol–gel preparation procedure, which resulted in the molecular level mixing of the starting materials and enabled a high degree of homogeneity to be obtained with uniform particles having a high surface area. Fig. 4(c)–(f) shows the distribution of metal ions in sample D containing carbon and the corresponding mapping area is shown in Fig. 4(b). The mapping of Mn (Fig. 4(c)) showed a similar intensity distribution to Ni and Fe, indicating that all of the elements are homogeneously mixed in the sample. Fig. 4(f) clearly demonstrates the presence of carbon with an even distribution on the surface of the powders. Sample D with a ratio of AA to metal ions of 1 M, which showed the best performance among the synthesized powders, was found to contain only 1.6 wt% of carbon after the synthesis by CHN analysis. As its content is low, the carbon is not uniformly distributed and cannot cover the entire surface of the particles, as confirmed in the HR-TEM images in Fig. 4(g) [28].

Table 1
Lattice parameter values of $Li_{1.2}(Mn_{0.32}Ni_{0.32}Fe_{0.16})O_2$.

Sample	a_h/nm	c_h/nm	*c*/*a*	I_{003}/I_{104}
Pristine	2.889	14.289	4.95	1.12
A	2.885	14.284	4.94	0.75
B	2.883	14.278	4.94	0.78
C	2.882	14.275	4.94	0.87
D	2.881	14.273	4.94	0.94

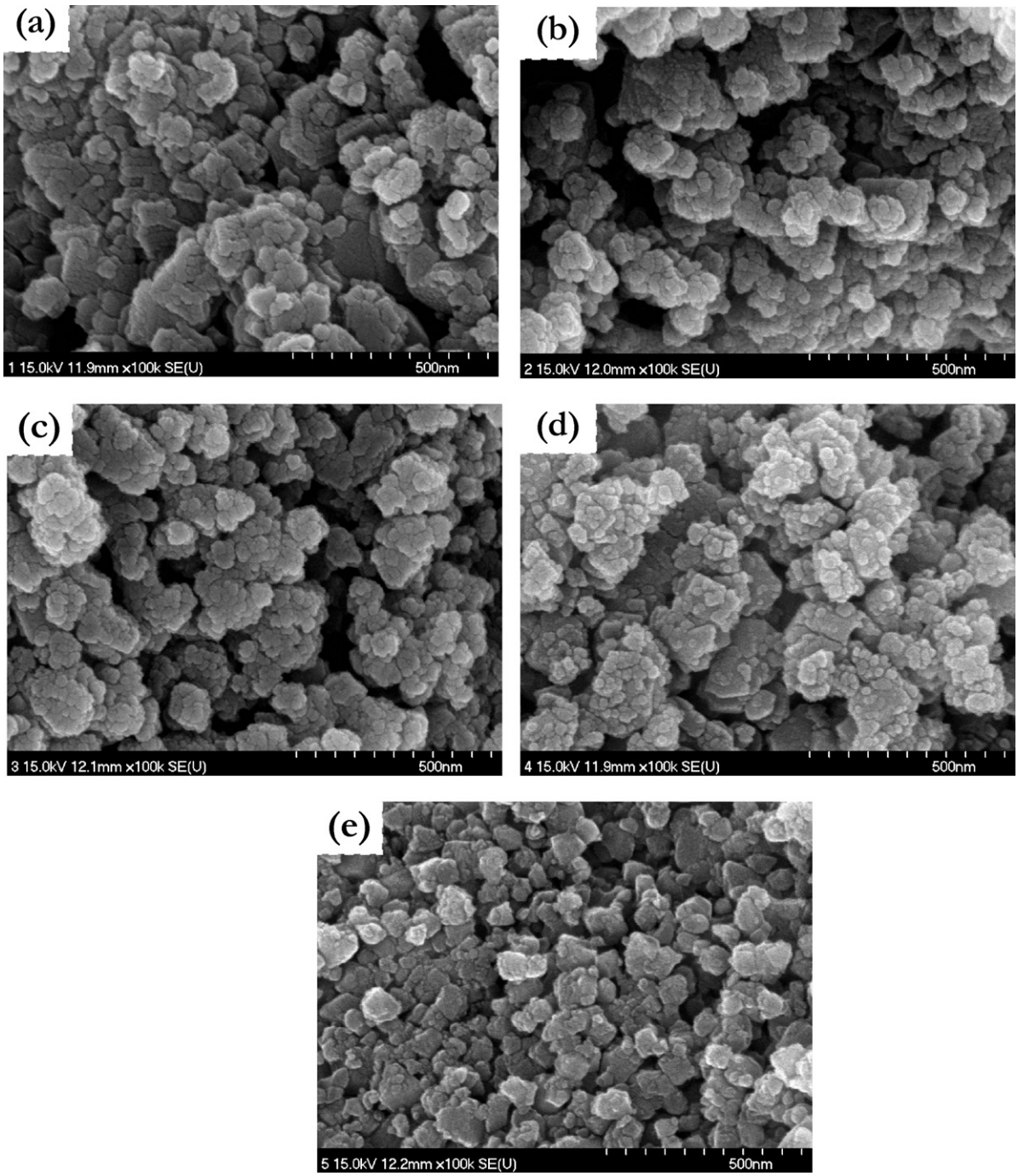

Fig. 3. SEM images of pristine and adipic acid assisted $Li_{1.2}(Mn_{0.32}Ni_{0.32}Fe_{0.16})O_2$ materials (a) pristine, (b) 0.25 M AA, (c) 0.5 M AA, (d) 0.75 M AA, and (e) 1 M AA concentrations.

A BET surface area analysis was also carried out to confirm the effect of AA on the surface area of the LMNFO powders. The analysis of the surface area is an important tool for the interpretation of the electrochemical performance, particularly in the case of Li_2MnO_3-based electrode materials, because samples with a large surface area exhibit better electrochemical behavior [23,29]. The specific surface areas of the pristine sample and samples A, B, C and D are about 4.44, 4.73, 4.87, 6.94 and 7.28 $m^2\,g^{-1}$, respectively. From the above measurements, it is obvious that the surface area increases with increasing amount of AA, which indirectly confirms that the chelating agent, adipic acid, played a vital role in hindering the aggregation of the particulates during calcination, increasing the surface area of the synthesized powders. The reason for the increase in the surface area and crystallinity of the material with increasing quantity of AA can be described as follows: it has been reported that AA not only acts as a chelating agent, but also provides the heat of combustion required for the preparation of highly crystalline powders [30–32]. Therefore, the high homogeneity of the precursor and a large amount of combustion heat is generated when a large amount of AA is used for the synthesis. The formation of a phase pure and lighter material, due to the large volume of voids formed by the evolution of CO and CO_2 gases during the thermal decomposition of AA. The swelling of the materials was observed even though the gel precursors with AA were calcined at a fixed temperature. In addition, their highly crystalline nature and high surface area lead to the complete participation (in other

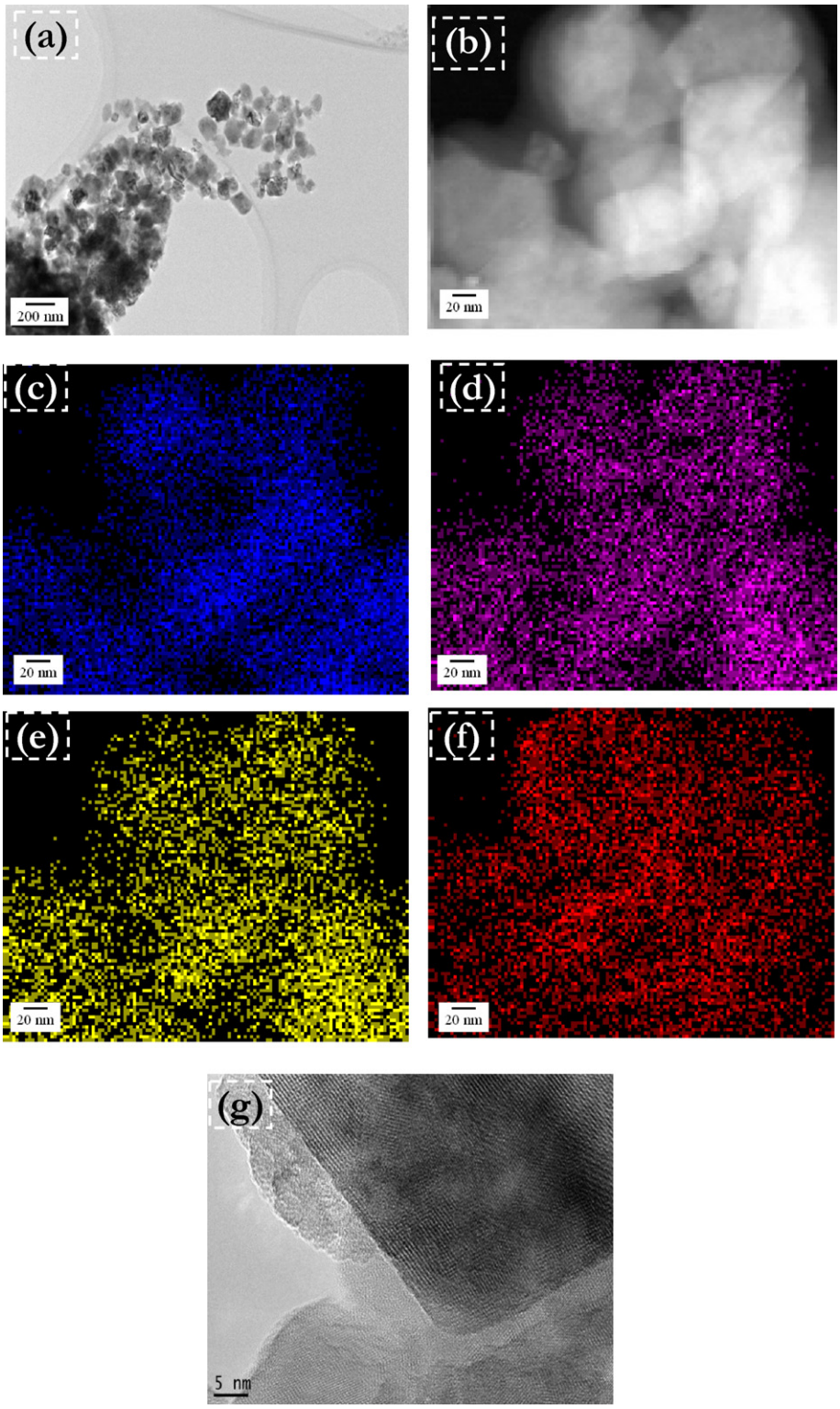

Fig. 4. TEM images of (a and b) 1 M adipic acid assisted $Li_{1.2}(Mn_{0.32}Ni_{0.32}Fe_{0.16})O_2$ particles, (c) mapping of Mn, (d) mapping of Ni, (e) mapping of Fe, (f) mapping of C, and (g) coating layer.

words, highly exposed contact area towards the electrolyte) of the materials during an electrochemical reaction.

The galvanostatic charge–discharge profile of the pristine material and samples A, B, C, and D are presented in Fig. 5. The cycling tests were carried out between 2 and 4.5 V vs. Li/Li^+ at a constant current density of 0.1 mA cm^{-2}. All of the synthesized samples exhibited smooth and monotonous curves, which is the typical behavior of layered materials and confirms the single phase reaction. During charging, the cell voltage started from open circuit voltage, rapidly increased to 3.7 V and then remained constant at 3.8 V where the oxidation of Ni^{2+} to Ni^{4+} occurred [33]. Since Mn^{4+} cannot be further oxidized to Mn^{5+}, it is believed that it did not take part in the electrochemical reaction [2]. Similar to Mn^{4+}, Fe^{3+} is also not oxidized to Fe^{4+} and is subsequently reduced during discharge,

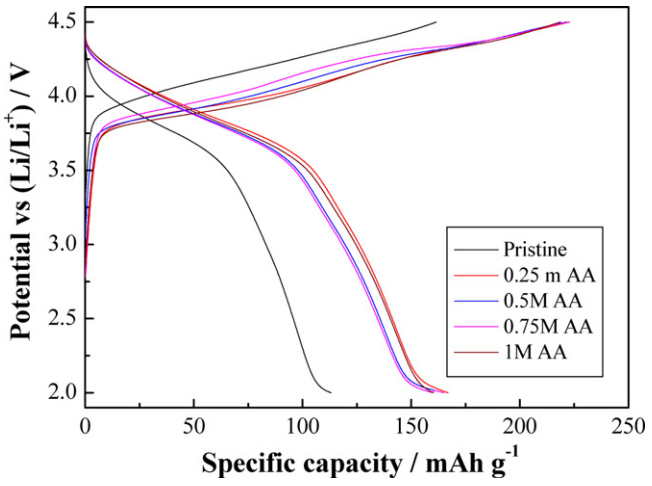

Fig. 5. Charge–discharge profiles of pristine $Li_{1.2}(Mn_{0.32}Ni_{0.32}Fe_{0.16})O_2$ and materials prepared with different AA ratios cycled between 2.0 and 4.5 V at a current density of 0.1 mA cm^{-2}.

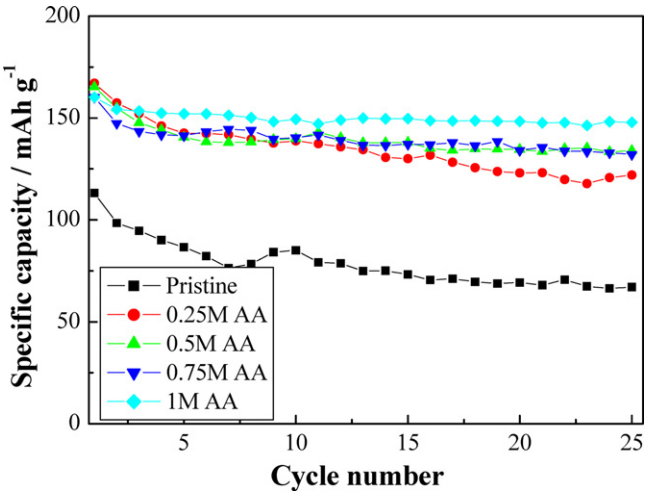

Fig. 6. Cycleability of pristine $Li_{1.2}(Mn_{0.32}Ni_{0.32}Fe_{0.16})O_2$ and materials prepared with different AA ratios for 25 cycles at room temperature.

as confirmed by the absence of an Fe^{3+}/Fe^{4+} redox plateau at ~4 V caused by the partial occupation of the transition layers of the α-$NaFeO_2$ type structure by the Fe ions [34,2]. In this solid solution consisting of $Li_{1.2}(Mn_{0.32}Ni_{0.32}Fe_{0.16})O_2$, both Mn and Fe simply act as the inactive matrix elements, which stabilize the crystal structure during the $Ni^{4+/2+}$ redox couple. Moreover, a small amount of Fe^{3+} ions (3b cation) on the Li layer could act as an activator, prohibiting faster Li^+ diffusion and resulting in slower Li_2O extraction from the layered structure (α-$NaFeO_2$) during the charging process, thus explaining the large discharge capacity value [34,35]. It can be seen from Fig. 5 that a large irreversible capacity loss (ICL) is observed for all of the samples tested. This may be ascribed to the oxidation of pre-existing Ni^{2+} ions which occupy the Li^+ layer and lead to the formation of an electrochemically inactive region in the electrode in the first cycle. From the 2nd cycle onwards, the columbic efficiency of the cell is over 99% and this is noticed for all of the samples tested. As shown in Fig. 5, the discharge capacity of the pristine material is as low as 113 mAh g^{-1} when compared with the other materials, which may be due to its higher charge transfer resistance. In other words, the materials prepared with different AA ratios delivered almost the same discharge capacity value of about 160 mAh g^{-1} with different cycling behavior. This improved capacity resulted from the addition of AA during the synthesis, which facilitated the formation of particles with a preferred surface morphology and enhanced the contact between the active materials, thereby improving the electrochemical performance. Nevertheless, the suppression of the elimination of oxides and lithium ion vacancies at the end of the first charge cycle is effectively circumvented by the presence of carbon, which resulted in lower ICL and subsequently increased the columbic efficiency after first cycle [36].

Fig. 6 presents the cycling performance of the Li/LMNFO cells with different proportions of AA at a current density of 0.1 mA cm^{-2} at room temperature. The Li/LMNFO cells with AA concentrations of 0, 0.25, 0.5, 0.75 and 1 M delivered initial discharge capacities of 113, 167, 165, 160 and 160 mAh g^{-1}, respectively. The cycling performance tests of the Li/LMNFO cells were conducted for up to 25 cycles at room temperature. The discharge capacity of all of the samples slowly decreased with increasing cycling number, which is probably due to small structural distortion and/or side reactions during the charge–discharge process. As far as the pristine material is concerned, the discharge capacity started to fade severely from 113 to 68 mAh g^{-1} at the end of the 25th cycle, which corresponds to a capacity retention of 60%. On the other hand, the adipic acid mediated $Li_{1.2}(Mn_{0.32}Ni_{0.32}Fe_{0.16})O_2$ powder showed better cycleability than the pristine sample. Discharge capacities of 109, 134, 132 and 148 mAh g^{-1} were observed for the cells with concentrations of AA of 0.25, 0.5, 0.75 and 1 M at the 25th cycle, respectively. The capacity retentions of samples A, B, C and D were found to be 65, 81, 82 and 92% after the 25th cycle, respectively. Among the adipic acid assisted powders, 1 M AA comprising $Li_{1.2}(Mn_{0.32}Ni_{0.32}Fe_{0.16})O_2$ (sample D) exhibited excellent capacity retention. These improved properties result from the high crystallinity of the particles with a relatively larger surface area, which was confirmed by the SEM and BET analyses. The high surface area of such evenly distributed nanocrystalline materials improved the electrochemical performance by shortening the diffusion length of the lithium ions. The suppressed development of an SEI layer gives rise to significantly improved cycling performance, which indicates the effect of AA on the cycleability, even with a small applied carbon content. The conductive carbon on the surface not only prevents the direct contact between the active cathode material and the electrolyte, but also provides pathways for electron transfer.

The rate capability is one of the important electrochemical properties of a lithium secondary battery, which is required for high power storage applications. In order to demonstrate the rate capability of the pristine and AA containing materials, the cells were cycled with various current rates from 0.03 to 1*3C* between 2 and 4.5 V and the results are presented in Fig. 7. As mentioned earlier, some fading of the discharge capacity profile is observed when the cells are cycled at lower current rates (0.03*C*). In Fig. 7, it can be seen that the discharge capacity slowly decreased with increasing current density, due to the polarization of the electrodes at high current. This increase in polarization with increasing current rate is believed to be due to the reduction in the time required for Li^+ ion intercalation into the crystal lattice and the fact that only the surface of the active material participates in the reaction. It can be seen from Fig. 7 that the material prepared with 1 M AA exhibited excellent electrochemical behavior with improved cycleability even at high current rates, whereas the pristine sample showed poor rate performance. This data reveals that the rate capability increased with increasing AA ratio, due to the improved electrical conductivity arising from the phase purity, uniformly distributed highly crystalline nanoparticles and the presence of carbon.

Cyclic voltammetry was conducted for the 1 M AA containing $Li_{1.2}(Mn_{0.32}Ni_{0.32}Fe_{0.16})O_2$ (sample D) to evaluate the redox potential of the transition metal ions during cycling. Fig. 8 represents the family of cyclic voltammetric traces (1, 2, 6 and 10th cycles) of sample D between 2 and 4.5 V at 0.5 mV s^{-1}, in which lithium acts as

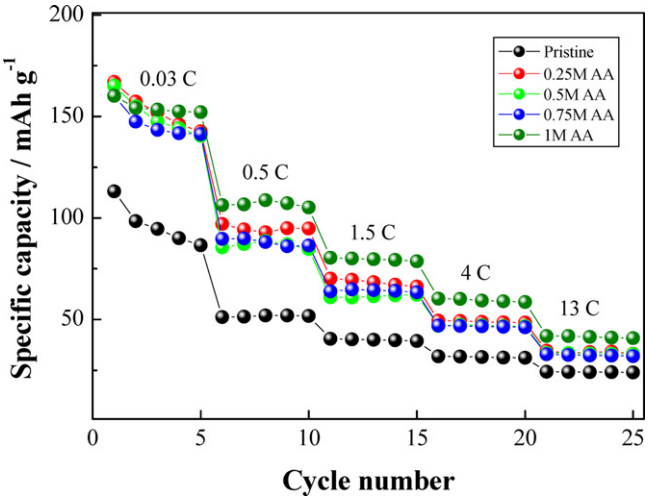

Fig. 7. Rate capability of pristine, 0.25 M AA, 0.5 M AA, 0.75 M AA, and 1 M adipic acid assisted $Li_{1.2}(Mn_{0.32}Ni_{0.32}Fe_{0.16})O_2$ samples at different current rates.

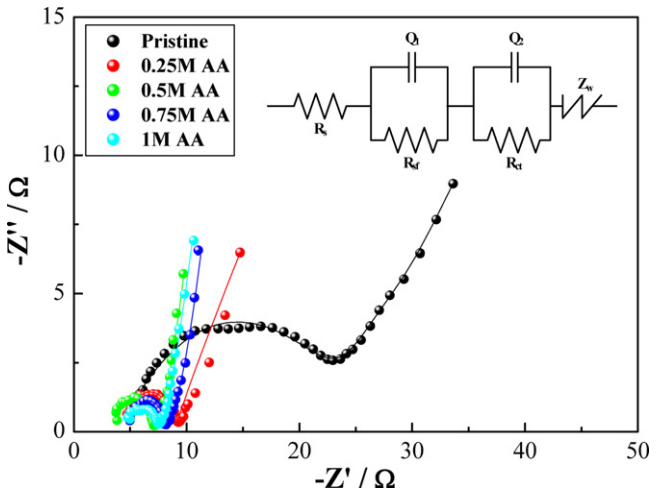

Fig. 9. EIS spectra of pristine and adipic acid assisted $Li_{1.2}(Mn_{0.32}Ni_{0.32}Fe_{0.16})O_2$ after cycling at current rates of 0.03*C* and 13*C*, respectively. The equivalent circuit is given in the inset.

the counter and reference electrodes. It can be seen that an anodic peak appears at around 4.2 V during charging and the corresponding cathode peak is seen at 3.6 V in the discharge process. According to an earlier report [12], the anodic peak at around 4.2 V corresponds to the oxidation of Ni^{2+} to Ni^{4+}. Furthermore, the absence of peaks at around 3 V indicates that the Mn^{4+}/Mn^{3+} redox reaction does not occur. This observation confirms that the Mn ions in our sample are electrochemically inactive and present in the 4+ state. Moreover, no transition of $Fe^{3+/4+}$ is observed throughout the region tested, which also confirms that the capacity obtained is due to the $Ni^{4+/2+}$ redox couple. As seen from the CV curves, the peak intensity became less sharp and shifted slightly towards the lower voltage region, whereas in the galvanostatic cycling no shift in the plateaus was noticed. The fading of the peak intensity can be attributed to the cation mixing in the first cycle and, thereafter, the CV curves of the 6th and 10th cycles almost overlap, which demonstrates the good reversibility of the Li^+ ions during insertion/extraction.

EIS studies were conducted to find the difference in the electrochemical performance and polarization effect between the pristine and AA assisted materials. The impedance data was recorded using a two electrode coin cell configuration and are presented in Fig. 9. The cells were initially charged and discharged at various current rates of 0.03*C* and 13*C*, respectively, which continuously cycled for 5 cycles each and then investigated with EIS. The small variation of the electrolyte resistance (R_s) observed in Fig. 9 can be neglected [37]. The EIS plots were fitted according to the equivalent circuit given in the inset of Fig. 9 and the parameters are summarized in Table 2. All of the EIS spectra consist of three regions: a semi-circle in the low and medium frequency regions and an inclined line in the high frequency region. The low frequency semicircle is related to the Li^+ ion migration resistance (R_{sf}) through the solid-electrolyte interfacial (SEI) film; the intermediate frequency semicircle is attributed to the charge transfer resistance (R_{ct}) in the cathode-electrolyte interface and the line inclined at approximately 45° to the real axis corresponds to lithium ion diffusion into the bulk of the electrode material. The semicircles in the low frequency region are broad and depressed, due to the overlap of the two separate semicircles. Nyquist spectra comprising two semicircles and a linear part, similar to those in the present study, have been reported for layered cathode materials [38]. It was found that the AA assisted cathodes have a relatively lower R_{sf} compared with the pristine one. One possible reason for this is the change in the interfacial structure of the materials after they are modified with AA, which may further influence the properties of the SEI layer, such as its thickness and density [39,40]. A much more obvious difference among all of the samples lies in the second semicircle in the medium frequency region (R_{ct}). It can be seen from Table 2 that the diameter of the semi-circle (i.e. R_{ct}) linearly decreased from 18.66 Ω to 3.2 Ω as the AA concentration increased. Among the samples, sample D delivered the lowest R_{ct} of about 3.2 Ω, which might be caused by its relatively faster ionic migration. The decrease in R_{ct} with increasing ratio of AA to metal ions clearly demonstrated the importance of both the electronic conductivity and the Li^+ diffusion ability for the excellent electrochemical behavior of the electrode

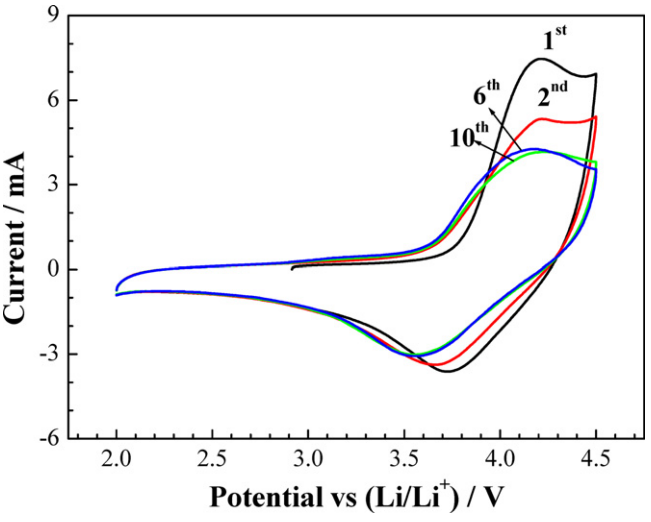

Fig. 8. Cyclic voltammograms of $Li_{1.2}(Mn_{0.32}Ni_{0.32}Fe_{0.16})O_2$ prepared with 1 M AA recorded between 2 and 4.5 V at 0.5 mV s^{-1}.

Table 2
EIS parameters of pristine and AA assisted materials obtained based on the equivalent circuit inserted in Fig. 9.

Sample	R_s/Ω	R_{sf}/Ω	R_{ct}/Ω
Pristine	5.40	6.53	18.66
A	4.67	2.23	4.36
B	3.83	1.68	3.79
C	4.95	1.52	3.44
D	4.74	0.88	3.20

materials during cycling at high current rates [41], which is well correlated with the charge/discharge cycling data.

4. Conclusions

Highly crystalline layered $Li_{1.2}(Mn_{0.32}Ni_{0.32}Fe_{0.16})O_2$ cathode materials with and without the presence of a chelating agent, adipic acid, were successfully synthesized through the conventional sol–gel method. The XRD results revealed that the use of a high concentration of chelating agent improved the crystalline nature of the layered compound. The galvanostatic profiles demonstrated that the presence of adipic acid during the synthesis played a vital role in increasing the surface area of the material and enabled a discharge capacity of $\sim$160 mAh g^{-1} to be delivered for all of the samples except for the bare compound. Among the samples, the material synthesized with 1 M adipic acid maintained 92% of its initial discharge capacity even after 25 cycles. The rate capability of the above material was improved compared with those of the pristine material and samples with other concentrations of adipic acid (0.25, 0.5 and 0.75 M), due to the increase in conductivity. These experimental results suggest that adipic acid mediated $Li_{1.2}(Mn_{0.32}Ni_{0.32}Fe_{0.16})O_2$ is an "eco-friendly" candidate for next generation cathode materials for lithium ion batteries.

Acknowledgments

This research work was financially supported by the Ministry of Knowledge Economy (MKE), Korea Institute for Advancement of Technology (KIAT) and Honam Leading Industry Office through the Leading Industry Development for Economic Region.

References

[1] R.J. Brodd, K.R. Bullock, R.A. Leising, R.L. Middaugh, J.R. Miller, E. Takeuchic, J. Electrochem. Soc. 151 (2004) K1.
[2] B. Ammundsen, J. Paulsen, Adv. Mater. 13 (2001) 943.
[3] G. Dutta, A. Manthiram, J.B. Goodenough, J. Solid State Chem. 96 (1992) 123.
[4] Y. Gao, M.V. Yakovleva, W.B. Ebner, Electrochem. Solid-State Lett. 1 (1998) 117.
[5] G. Vitins, K. West, J. Electrochem. Soc. 144 (1997) 2587.
[6] O.K. Park, Y. Cho, S. Lee, H.C. Yoo, H.K. Song, J. Cho, Energy Environ. Sci. 4 (2011) 1621.
[7] Y. Makimura, T. Ohzuku, J. Power Sources 119–121 (2003) 156.
[8] T. Ohzuku, Y. Makimura, Chem. Lett. 30 (2001) 642.
[9] S. Jouanneau, K.W. Eberman, L.J. Krause, J.R. Dahn, J. Electrochem. Soc. 150 (2003) A1637.
[10] A.D. Robertson, P.G. Bruce, Chem. Commun. 23 (2002) 2790.
[11] A.D. Robertson, P.G. Bruce, Chem. Mater. 15 (2003) 1984.
[12] Z. Lu, J.R. Dahn, J. Electrochem. Soc. 149 (2002) A1454.
[13] L. Zhang, H. Noguchi, M. Yoshio, J. Power Sources 110 (2002) 57.
[14] Y. Sun, Y. Shiosaki, Y. Xia, H. Noguchi, J. Power Sources 159 (2006) 1353.
[15] M.M. Thackeray, S.H. Kang, C.S. Johnson, J.T. Vaughey, R. Benedeka, S.A. Hackney, J. Mater. Chem. 17 (2007) 3112.
[16] Y. Sun, C. Ouyang, Z. Wang, X. Huang, L. Chen, J. Electrochem. Soc. 151 (2004) A504.
[17] P.S. Whitfield, S. Niketic, I.J. Davidson, J. Power Sources 146 (2005) 617.
[18] L. Zhang, K. Takada, N. Ohta, K. Fukuda, T. Sasaki, J. Power Sources 146 (2005) 598.
[19] N. Yabuuchi, K. Yoshii, S.T. Myung, I. Nakai, S. Komaba, J. Am. Chem. Soc. 133 (2011) 4404.
[20] S.S. Shin, Y.K. Sun, K. Amine, J. Power Sources 112 (2002) 634.
[21] M. Ma, N.A. Chernova, B.H. Toby, P. Zavalij, M.S. Whittingham, J. Power Sources 165 (2007) 517.
[22] J. Li, J. Li, J. Luo, L. Wang, X. He, Int. J. Electrochem. Sci. 6 (2011) 1550.
[23] M. Tabuchi, Y. Nabeshima, K. Ado, M. Shikano, H. Kageyama, K. Tatsumi, J. Power Sources 174 (2007) 554.
[24] M. Tabuchi, Y. Nabeshima, T. Takeuchi, H. Kageyama, K. Tatsumi, J. Akimoto, H. Shibuya, J. Imaizumi, J. Power Sources 196 (2011) 3611.
[25] G.T.K. Fey, J.G. Chen, Z.F. Wang, H.Z. Yang, T.P. Kumar, Mater. Chem. Phys. 87 (2004) 246.
[26] T. Ohzuku, A. Ueda, M. Nagayama, J. Electrochem. Soc. 140 (1993) 1862.
[27] C. Suryanarayana, C.C. Koch, Hyperfine Interact. 130 (2000) 5.
[28] R. Guo, P. Shi, X. Cheng, C. Du, J. Alloys Compd. 473 (2009) 53.
[29] D. Yu, K. Yanagida, K. Kato, H. Nakamura, J. Electrochem. Soc. 156 (2009) A417.
[30] Y.K. Sun, I.H. Oh, S.-A. Hong, J. Mater. Sci. 31 (1996) 3617.
[31] Y.K. Sun, I.-H. Oh, J. Mater. Sci. Lett. 16 (1997) 30.
[32] Y.S. Lee, Y.K. Sun, K.S. Nahm, Solid State Ionics 109 (1998) 285.
[33] Y. Koyama, I. Tanaka, H. Adachi, Y. Makimura, T. Ohzuku, J. Power Sources 119 (2003) 644.
[34] M. Tabuchi, A. Nakashima, H. Shigemura, K. Ado, H. Kobayashi, H. Sakaebe, H. Kageyama, M. Kohzaki, A. Hirano, R. Kanno, J. Electrochem. Soc. 149 (2002) A509.
[35] C. Delmas, G. Prado, A. Rougier, E. Suard, L. Fournès, Solid State Ionics 135 (2000) 71.
[36] Q.Y. Wang, J. Liu, A.V. Murugan, A. Manthiram, J. Mater. Chem. 19 (2009) 4965.
[37] J. Liu, A. Manthiram, Chem. Mater. 21 (2009) 1695.
[38] D. Aurbach, M.D. Levi, E. Levi, A. Schechter, The Electrochem. Soc., Pennington, 1997, p. 124.
[39] D. Aurbach, B. Markovsky, A. Rodkin, M. Cojocaru, E. Levi, H.J. Kim, Electrochim. Acta 47 (2002) 1899.
[40] G.T.K. Fey, P. Muralidharan, Y.D. Cho, J. Power Sources 160 (2006) 1294.
[41] H. Liu, C. Li, H. Zhang, L. Fu, Y. Wu, H. Wu, J. Power Sources 159 (2006) 717.